Available online at www.sciencedirect.com
SCIENCE DIRECT®
Journal of Solid State Chemistry 176 (2003) 243–249
JOURNAL OF SOLID STATE CHEMISTRY
http://elsevier.com/locate/jssc

Molecular hexagonal perovskite: a new type of organic–inorganic hybrid conductor

T. Naito* and T. Inabe

Division of Chemistry, Graduate School of Science, Hokkaido University, Kita 10, Nishi 8, Kita-ku, Sapporo, Hokkaido 060-0810, Japan

Received 15 April 2003; received in revised form 11 July 2003; accepted 23 July 2003

Abstract

An organic charge-transfer (CT) salt $(BEDT\text{-}TTF)_3(MnCl_3)_2(C_2H_5OH)_2$ has been synthesized by a standard electrochemical method. The crystal data are monoclinic, $C2/c$ (#15), $a = 38.863(4)$ Å, $b = 6.716(1)$ Å, $c = 23.608(3)$ Å, $\beta = 115.007(3)^\circ$, $V = 5584(1)$ Å^3, and $Z = 4$. The structure consists of one-dimensional (1D) infinite $\{[MnCl_3]^-\}_\infty$ magnetic chains and two-dimensional (2D) organic conduction pathways. The former consists of face-sharing octahedra of manganese chloride complex ions, and dominates the magnetic properties of this compound. Such a feature of the crystal structure closely relates to transition metal hexagonal perovskite compounds, all of which are known for frustrated triangular lattices comprised of weakly interacting 1D magnetic chains. The new compound exhibits a high conductivity down to 4 K.

1. Introduction

The conducting and/or magnetic materials based on charge-transfer (CT) salts of molecular crystals have been intensively studied for more than 20 years [1]. Now there are a great number of examples of synthetic ferromagnets, metals and superconductors based on organic and/or metal complex molecules. As for the next goal to achieve for the molecular (super) conductors, worldwide efforts have been focused to develop combined functional materials such as ferromagnetic superconductors. Realization of such kinds of molecular materials are also evidently important for application as various types of nano-devices. One of the straightforward ways to obtain magnetic conducting molecular materials is to synthesize molecular CT salts containing transition metal ions [2–12]. Among the constituent species of molecular conductors, BEDT-TTF (ET; Scheme 1) is best known to produce a wide variety of conducting CT salts with various types of counter anions [13]. Additionally one can find many superconducting ET salts with polymerized metal (pseudo)-halide complex anions [1,13]. Polymerized transition metal complex ions generally exhibit strong magnetic interactions between the metal centers, which is advantageous for interesting magnetic properties. Therefore, CT salts of ET and polymerized transition metal complex ions can be the material of choice for the molecular magnetic (super)conductors. In the course of pursuit of such materials the title compound was obtained. Although there are a number of ET-based conducting CT salts with polymerized metal complex anions, the title compounds is an important example because it occupies a middle position between the molecular CT conductors and (hexagonal) perovskite type magnetic materials. Some related pioneering work has been done [14]. The hexagonal perovskites have the same general formula ABX_3 with the well-known cubic perovskites, yet do have totally different crystal structures from the latter [15]. All of the known hexagonal perovskite transition metal compounds are insulating, however, they exhibit unusual magnetic behavior due to their triangular lattices comprised of the 1D antiferromagnetic chains [16–18]. With maintaining such magnetic structure, the title compound is highly conductive down to 4 K. In this paper we report

*Corresponding author. Present address: Creative Research Initiative "Sousei", Division of Innovative Research, Hokkaido University, Sapporo, Hokkaido 060-0810, Japan. Fax: +81-11-7063534.
E-mail address: tnaito@sci.hokudai.ac.jp (T. Naito).

0022-4596/$ - see front matter © 2003 Elsevier Inc. All rights reserved.
doi:10.1016/S0022-4596(03)00418-3

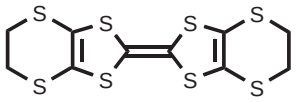

"ET"

Scheme 1.

on the unique crystal structure, electrical and magnetic properties.

2. Experimental

2.1. Synthesis

Purest grade reagents commercially available were purchased and used as received; ET and $(C_6H_5)_4P \cdot I$ (Tokyo Chemical Industry Co., Ltd.), $KMnO_4$ (Koso Chemical Co., Ltd.) and 1,1,2-$C_2H_3Cl_3$ (Kanto Chemical Co., Inc.), respectively. All the other reagents were purchased from Wako Pure Chemical Industries, Ltd. The Mn-clusters $[Mn_{12}O_{12}(C_6H_5COO)_{16}(H_2O)_4] \cdot C_6H_5COOH \cdot CH_2Cl_2$ [19] and $(C_6H_5)_4P[Mn_{12}O_{12}(C_6H_5COO)_{16}(H_2O)_4]$ [20] were prepared starting from $[Mn_{12}O_{12}(CH_3COO)_{16}(H_2O)_4] \cdot 2CH_3COOH \cdot 4H_2O$ [21] by reported methods. The single crystals of $(ET)_3(MnCl_3)_2(C_2H_5OH)_2$ were obtained by the electrolysis of ET (22 mg) in 1,1,2-$C_2H_3Cl_3$ containing 10 vol% of C_2H_5OH (50 mL in total) with the Mn-clusters $[Mn_{12}O_{12}(C_6H_5COO)_{16}(H_2O)_4] \cdot C_6H_5COOH \cdot CH_2Cl_2$ (6 mg) and $(C_6H_5)_4P[Mn_{12}O_{12}(C_6H_5COO)_{16}(H_2O)_4]$ (39 mg) at 20°C under a nitrogen atmosphere. A standard cell for electro-crystallization with a grass frit of fine porosity [22] and platinum wires as electrodes (each 1 mm thick in diameter) were used. The current was maintained at 2.5 μA for a month. The voltage between the two platinum electrodes was initially 8–10 V. No reference electrode was used.

2.2. X-ray structural analysis

For the X-ray structural analysis a selected single crystal (H:; L:; B:) 0.625 mm × 0.125 mm × 0.125 mm was glued to a glass fiber. The reflection data collection was carried out with a Rigaku R-AXIS RAPID Imaging Plate area detector with graphite monochromated Mo$K\alpha$ radiation ($\lambda = 0.7107$ Å) at RT. The intensities were corrected for Lorentz and polarization effects. Empirical absorption correction was applied. The structure was solved by a direct method [23], and the hydrogen atoms were placed at the calculated ideal positions. A full-matrix least-squares technique on F with anisotropic thermal parameters for non-hydrogen atoms and isotropic ones for hydrogen atoms was employed for the structure refinement. Hydrogen atoms were included but not refined. Atom scattering factors were taken from the literature [24]. The values for the mass attenuation coefficients were those of Creagh and Hubbell [25]. All calculations were performed using teXsan crystallographic software package (Molecular Structure Corporation, The Woodlands, TX, 77381). The structural views were produced using ORTEP-3 for Windows [26]. All the measurements of physical properties below were carried out immediately after the filtration of the single crystals. They were quickly identified to be the desired product of good quality by X-ray photographs using a Rigaku Imaging Plate.

2.3. Resistivity measurements

The electrical resistivity was measured on a single crystal (parallelepiped) with a typical size of 1 mm × 0.1 mm × 0.1 mm. A standard direct-current 4-probe method was used. The electrical leads were gold wires (each 20 μm in diameter). They were attached to the specimen with gold paint (No. 8560, Tokuriki). The current was applied along the b-axis on the most developed crystal facet, which was parallel to the bc-plane, i.e., the conduction plane. The resistivity measurements were carried out using a computer-controlled cryogenic refrigerator system. Linearity between applied current and observed voltage drop in the specimen was checked at the start of the measurement. The cooling or heating rates were 1 K min^{-1} (300–50 K) or 0.5 K min^{-1} (50–4.2 K) and the temperature-variation-rate dependence was not examined. The measurement started at RT, and turned to heating at 4.2 K after the temperature was kept at 4.2 K for 30 min for thermal equilibrium of the whole system. Other heating/cooling patterns were not examined.

2.4. Magnetic susceptibility

For magnetic susceptibility measurements, a few mg of single crystals (ca. 20–30 in number) were selected and set in a SQUID susceptometer MPMS-5S (Quantum Design) with field strengths of 0.8 and 0.1 T. The results were independent of the field strength. The examined temperature range was 1.8–300 K. The data were taken at every 0.5, 1, 2, 5 or 10 K depending on the temperature range. The linearity of magnetization up to ±5.0 T was checked at 1.8 K at 1000 Oe intervals, and no hysteresis nor saturation was observed. The diamagnetic correction was carried out using the observed values for the ET molecule (-2.18×10^{-4} cgs emu mol^{-1}) and the Pascal law for the remaining species. Field cooling (FC) and zero field cooling (ZFC) were both measured and the results were identical between the two processes. The cooling/heating-rate was 1–1.5 K min^{-1}. The rate-dependence was not observed.

2.5. ESR spectra

The electron spin resonance spectra (X-band; 9.3 GHz) were measured on the single crystal in the temperature range 3.5–300 K using an EMX EPR Spectrometer (Bruker) equipped with a continuous flow cryostat ESR 900 (Oxford). The measurement was carried out on several samples under different conditions.

2.6. Band calculation

The extended Hückel tight-binding band calculation was carried out using a program package written by Mori et al. [27].

3. Results and discussion

3.1. Crystal structure

The asymmetric unit contains one and a half ET molecules, a $MnCl_3$ ion and an ethanol molecule. Summary of crystal structure determination listing is given in Table 1. The selected bond lengths and angles are tabulated in Table 2. The atom numbering scheme is depicted as Fig. 1. Crystallographic data (excluding structure factors) for the structure reported in this paper have been deposited with the Cambridge Crystallographic Data Centre as supplementary publication No. CCDC-200484. Copies of the data can be obtained free of charge on application to CCDC, 12 Union Road, Cambridge CB2 1EZ, UK (fax: +44-1223-336-033; mailto:deposit@ccdc.cam.ac.uk). The X-ray structural analysis proves that it contains one-dimensional (1D) chains of polymerized manganese chloride anion running along the *b*-axis (Fig. 2a). Closer examination shows that the infinite chains consist of face-shared octahedral $[MnCl_6]^{4-}$ ions (Fig. 2b). The structural features of the infinite chain are quite similar to that of linear chain antiferromagnets such as $[(CH_3)_4N][MnCl_3]$ [28]. The bond lengths, (Mn(1)–Cl(1) 2.529(4), Mn(1)–Cl(1)* 2.570(4), Mn(1)–Cl(2) 2.601(5), Mn(1)–Cl(2)* 2.503(7), Mn(1)–Cl(3) 2.568(5), and Mn(1)–Cl(3)* 2.568(5) Å) are almost equal or slightly shorter than the corresponding ones in $[(CH_3)_4N][MnCl_3]$ [29], which leads to a trigonal elongation of the octahedron about the manganese atom. However, the bond angles (81.9(2)°, 96.6(2)° and 80.8(2)°) are slightly different from those in $[(CH_3)_4N][MnCl_3]$ [29]. This results in much shorter non-bonded contacts between chlorine atoms and between manganese atoms (Cl···Cl; 3.447(5) Å along the chain and 3.287(7) Å between the adjacent Cl atoms on the chain, and the neighboring Mn···Mn; 3.3585(1) Å along the chain). The manganese chloride (Mn–Cl) chains form insulating sheets with ethanol molecules, which are, in turn, inserted between the chains. The ethanol molecules, by way of weak head-to-tail hydrogen-bonding OH–C, display a dimer-like structure resembling a dioxane molecule. X-ray analysis clearly demonstrates the absence of disordered atoms in the unit cell. Nevertheless, there may be a deficiency in the ethanol sites due to gradual evaporation of the ethanol molecules. Between one S and one Cl atom there is an atomic contact (Cl···S; 3.524(4) Å) shorter than the sum of each van der Waals radius ($r_{Cl} + r_S = 3.650$ Å).

From experimental results discussed later, it has been established that the Mn ion takes +2 oxidation state and that all the ET species have an equal charge of +2/3. In perovskite compounds with a bulky (e.g., $(CH_3)_4N^+$) monocation *A*, the octahedra of metal complex anions in ABX_3 can be arranged into infinite 1D chains, which is a totally different crystal structure from the well known cubic or layered perovskites. In such a case the whole crystal structure often takes hexagonal symmetry. Therefore such a group of compounds are called *hexagonal perovskites* [15]. The hexagonal perovskites consist of 1D infinite chains of face-shared octahedra and large monocations separating the chains. The arrangement of chemical species in $(ET)_3(MnCl_3)_2(C_2H_5OH)_2$ actually share substantial

Table 1
Summary for crystallographic experimental details

Empirical formula	$C_{34}H_{36}O_2S_{24}Cl_6Mn_2$
Formula weight *M*	1568.69
Crystal color, habit	Black, needle
Crystal dimensions/(mm^3)	$0.62 \times 0.12 \times 0.12$
Crystal system	Monoclinic
Space group	$C2/c$ (#15)
Lattice type	C-centered
a (Å)	38.863(4)
b (Å)	6.716(1)
c (Å)	23.608(3)
β	115.007(3)
V (Å)^3	5584(1)
Z	4
T (°C)	23 ± 1
D_{calc} (g cm^3)	1.866
F_{000}	3168.00
μ (Mo$K\alpha$) (cm^{-1})	16.72
$2\theta_{max}$ (deg)	55.0
No. of reflections measured	Total: 16255 Unique: 5939 ($R_{int} = 0.092$)
Corrections	Lorentz-polarization Absorption (trans. factors: 0.5636–1.5515)
Structure Solution	Direct methods (SIR92)
Refinement	Full-matrix least-squares on F
Function minimized	$\sum w(\|F_o\| - \|F_c\|)^2$
Least-squares weights	$1/\sigma^2(F_o) = 4F_o^2/\sigma^2(F_o^2)$
No. variables	307
Reflection/parameter ratio	19.35
Residuals[a]: *R*; R_w	0.195; 0.066

[a] Both for all data.

Table 2
Selected bond lengths (Å) and angles (deg) in $(BEDT–TTF)_3(MnCl_3)_2(C_2H_5OH)_2$

Mn(1)–Cl(1)	2.529(4)	Mn(1)–Cl(1)[a]	2.570(4)	Mn(1)–Cl(2)[a]	2.503(7)
Mn(1)–Cl(3)[a]	2.568(5)	S(1)–C(1)	1.80(1)	S(1)–C(3)	1.69(1)
S(2)–C(2)	1.76(1)	S(2)–C(4)	1.71(1)	S(3)–C(3)	1.77(1)
S(3)–C(5)	1.77(1)	S(4)–C(4)	1.79(1)	S(4)–C(5)	1.72(1)
S(5)–C(6)	1.70(1)	S(5)–C(7)	1.74(1)	S(6)–C(6)	1.76(1)
S(6)–C(8)	1.82(1)	S(7)–C(7)	1.72(1)	S(7)–C(9)	1.76(2)
S(8)–C(8)	1.71(1)	S(8)–C(10)	1.80(1)	S(9)–C(11)	1.80(1)
S(9)–C(13)	1.70(1)	S(10)–C(12)	1.83(1)	S(10)–C(14)	1.72(1)
S(11)–C(13)	1.76(1)	S(11)–C(15)	1.71(1)	S(12)–C(14)	1.80(1)
S(12)–C(15)	1.71(1)	O–C(17)[b]	1.6(1)	C(1)–C(2)	1.53(2)
C(3)–C(4)	1.38(1)	C(5)–C(6)	1.34(1)	C(7)–C(8)	1.35(1)
C(9)–C(10)	1.25(2)	C(11)–C(12)	1.34(2)	C(13)–C(14)	1.34(2)
C(15)–C(15)[c]	1.40(2)	C(16)–C(17)	1.47(5)		
Cl(1)–Mn(1)[a]–Cl(1)	178.9(2)	Cl(1)–Mn(1)[a]–Cl(2)	98.9(2)		
Cl(1)–Mn(1)[a]–Cl(3)	96.6(2)	Cl(1)[a]–Mn(1)[a]–Cl(2)	81.9(2)		
Cl(1)[d]–Mn(1)[a]–Cl(3)	84.2(1)	Cl(2)[a]–Mn(1)[a]–Cl(3)	80.8(2)		
Mn(1)–Cl(1)[d]–Mn(1)	82.39(8)				

[a] Symmetry operations: $1/2-x$, $-1/2-y$, $-z$.
[b] Symmetry operations: $1/2+x$, $1/2-y$, $1/2+z$.
[c] Symmetry operations: $x+1$, $-y$, $1/2+z$.
[d] Symmetry operations: $1/2-x$, $1/2-y$, $-z$.

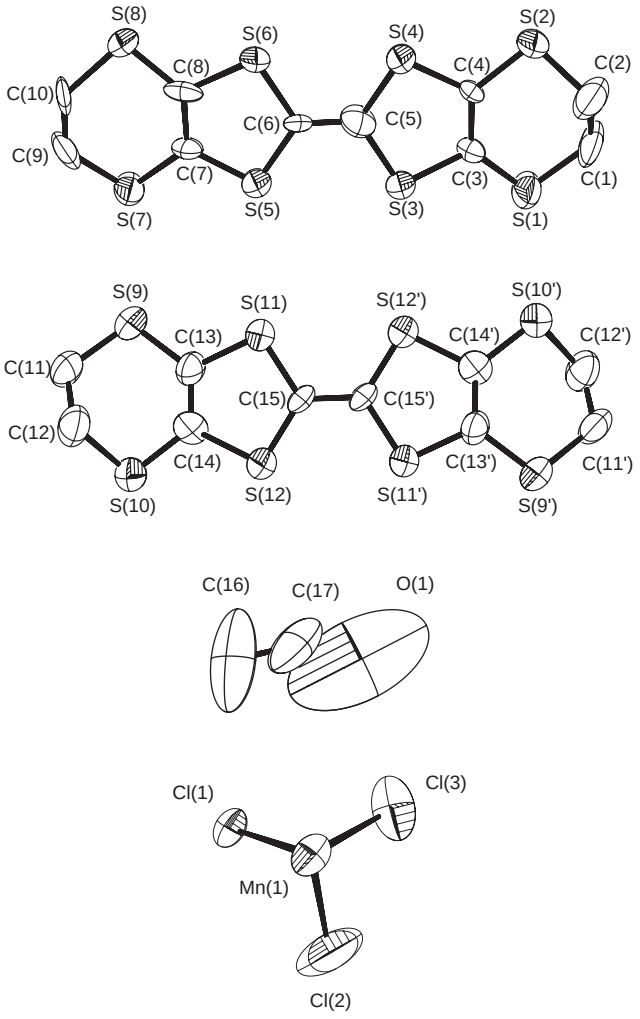

Fig. 1. Atom numbering scheme. Hydrogen atoms are omitted for clarity.

structural features with the hexagonal perovskites, though the crystal symmetry does not belong to the hexagonal system.

The ET molecules stack along the *c*-axis in a zigzag way with a sixfold periodicity (Figs. 2a and b). The long axes of each two neighboring ET molecules make an angle of 33° or 37° (Fig. 2c). Every two neighboring ET molecules also deviate from each other along the long molecular axes by about a half of the diameter of the five-membered (1,3-dithiole) ring ($\sim$1.66 Å). The ET arrangement in the *bc*-plane is conventionally called α'-type [30] (Fig. 3). There are many inter- and intracolumnar short S$\cdots$S atomic contacts ($\leqslant$3.70 Å) between the adjacent ET molecules. As a result the ET molecules apparently form two-dimensional (2D) sheets in the *bc*-plane.

3.2. Physical properties

3.2.1. ESR results

In inorganic or ionic perovskites, the cation *A* part is closed-shell and simply a "charge-reservoir" [31], and thus does not play a decisive role in their physical properties. The hybrid-type compound, however, presents a striking contrast to the inorganic perovskites. The cation *A* part (i.e., the ET sheet) plays an important role as the conduction sheet in this material. On the other hand the infinite Mn–Cl chains dominate the magnetic properties as well as those of ionic hexagonal perovskites. In short, the conducting and magnetic properties are separated into two parts in the crystal; ET sheets and Mn–Cl chains, respectively. Furthermore, the magnetic properties suggested a significant $\pi-d$ interaction between them (see below). In most of the organic

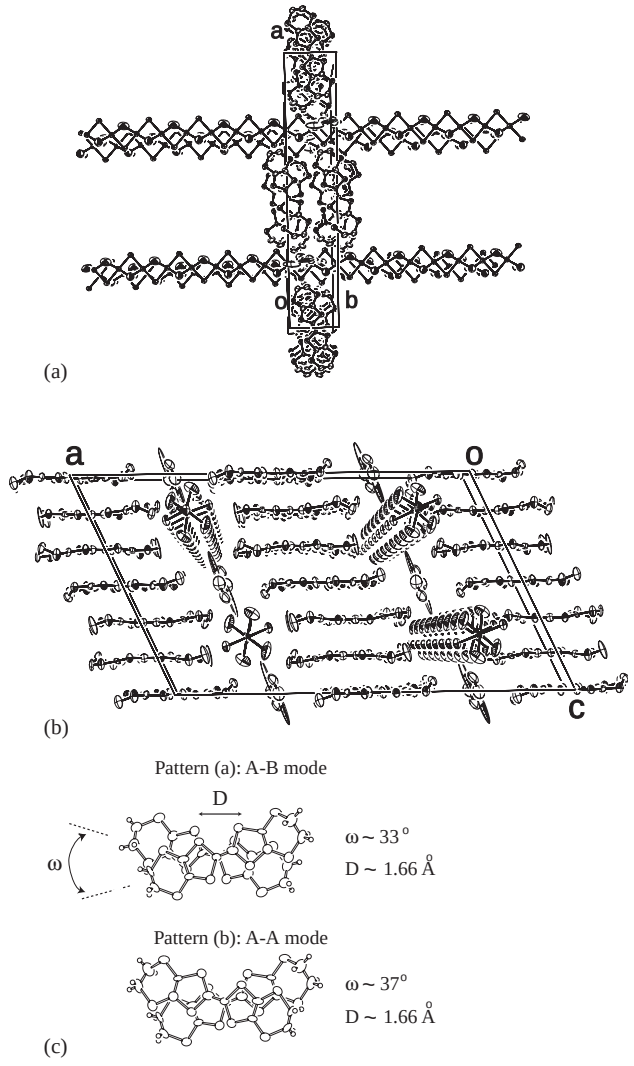

Fig. 2. (a) Unit cell viewed down along the *c*-axis and (b) viewed down along the *b*-axis. (c) Two molecular overlapping modes of ET. Hydrogen atoms are omitted for clarity except in (c).

molecular CT salts such interaction is negligibly small [6,9]. In these cases, each type of unpaired electrons, i.e., conduction and localized electrons, can be easily and separately detected by ESR measurements [2,3]. Inversely if the interaction is too strong, an ESR spectrum will not be observed [32]. This is because the very strong interaction should make the relaxation times too short to allow the observation of an ESR spectrum. In the polymerized metal complex species, for example, a strong exchange interaction between the adjacent metal centers often make their own spins undetectable in ESR. In the case of $(ET)_3(MnCl_3)_2(C_2H_5OH)_2$ no clear ESR signal was observed down to 3.5 K. The presence of strong exchange in the Mn chains could account for the lack of an ESR signal of the *d-spins*, but could not that of the *π-spins*. At present no explanation on this point is available.

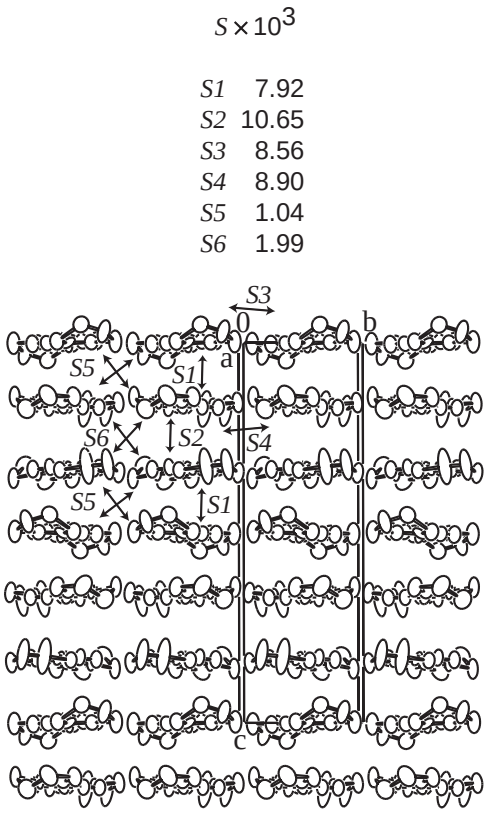

Fig. 3. Molecular arrangement of ET in the *bc*-plane with calculated overlap integrals (*S*'s) (due to the symmetry, crossed arrows are equivalent in *S*5 and *S*6, respectively).

3.2.2. Magnetic susceptibility

The temperature dependence of the magnetic susceptibility is shown in Fig. 4. An obvious feature is a small plateau around 20 K. This kind of behavior is often associated with 1D antiferromagnetic systems. In the curve-fitting analysis of the susceptibility we used a modified Bonner–Fisher [33] and a Curie–Weiss model. The former model can describe the intrinsic nature of an idealized 1D antiferromagnetic chain, while the latter is meant for weakly interacting spins from lattice defects and impurities. An increase in the susceptibility at low temperature is commonly observed in similar compounds [16], and was attributed to impurities. The parameters obtained are as follows; the magnitude of antiferromagnetic interaction in the 1D chain $J/k_B = -35.8$ K, the Curie constant describing the amount of spins on the manganese atom $C_{Mn} = 8.75$ emu K formula^{-1}, and that of the lattice defects $C = 0.27$ emu K formula^{-1}, the Weiss temperature corresponding to the magnetic interaction between spins from the lattice defects $\theta = -1.9$ K. The measured Curie constant C_{Mn} is 100% of the theoretically expected value of the high spin Mn(II) atoms per formula ($2 \times \mathrm{Mn}(S = 5/2)$). The Curie constant C is 3.1% of C_{Mn}, which is quite high but comparable with

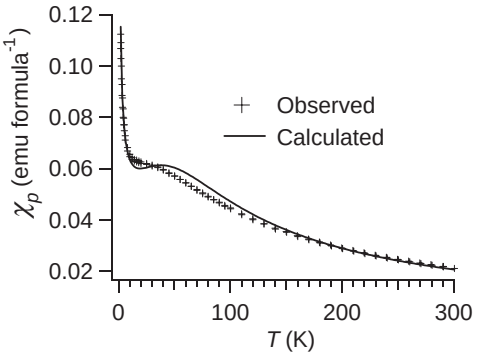

Fig. 4. Temperature (T) dependence of the magnetic susceptibility (χ_p) as χ_p vs. T plot. Electromagnetic unit (emu) is used, and χ_p is described per one mole of $(ET)_3(MnCl_3)_2(C_2H_5OH)_2$. A thin line describes the calculated one as a sum of the modified Bonner–Fisher and Curie–Weiss models (see text).

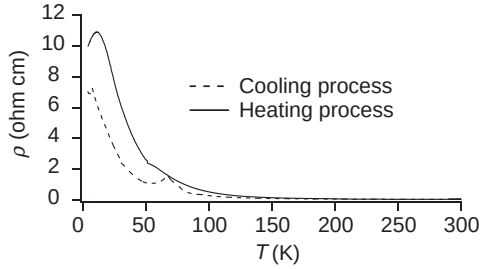

Fig. 5. Temperature dependence of the resistivity (ρ) along the b-axis.

those of hexagonal perovskite compounds [16]. Therefore, the magnetic behavior is practically reproduced by taking solely the spins on the Mn ions into consideration. This suggests that the contribution from the conduction electrons should be of Pauli paramagnetism. Pauli paramagnetism is a characteristic magnetism of conduction electrons in a metal. It is usually temperature-independent and smaller by some orders of magnitude than those of localized spins. Thus, the magnetic behavior of the π-spins on the ET radical could be metallic. Further study is evidently required to elucidate the magnetic behavior. In this new compound the situation could be clearer under high pressure, because then lattice shrinkage is anticipated. Generally speaking, the effect of high pressure on molecular crystals is to cause the emergence of intriguing physical properties owing to their lattice softness and flexibility.

3.2.3. Electrical resistivity

This salt exhibits very low resistivity along the b-axis down to 4 K (Fig. 5). The resistivity at RT was 0.04 Ω cm. On lowering the temperature the salt exhibited a gradually increasing resistivity, i.e., weakly semiconducting behavior. Still, it retained resistivity as low as ~10 Ω cm down to 4 K. A cusp-type maximum appeared at 67 K. A switching behavior (7 Ω cm ↔ 10 Ω cm) at 4 K was followed by a large hysteresis with a round maximum at 10 K. Such an unusual electrical behavior resembles that of a related material β''-$(ET)_3(MnCl_4)(1,1,2\text{-}C_2H_3Cl_3)$ [9]. In the case of β''-$(ET)_3(MnCl_4)(1,1,2\text{-}C_2H_3Cl_3)$, the unusual electrical behavior was attributed to the structural phase transition around 40–60 K based on a series of X-ray oscillation photographs. The phase transition was easily suppressed under high pressure of 3–5 kbar, and a clear metallic behavior ($\partial\rho/\partial T > 0$) without a resistivity maximum nor hysteresis was observed. In the case of $(ET)_3(MnCl_3)_2(C_2H_5OH)_2$, the origin of the electrical behavior at low temperature remains to be clarified. This high conductivity provides a dividing line between this and the known transition metal hexagonal perovskite compounds. The latter are all magnetic insulators [16]. The origin of such a difference is simple. It lies in the addition of the organic conduction pathway to the insulating inorganic magnetic chains. It enables a new situation in which low resistivity and interesting magnetic properties can coexist. Even in the inorganic *conducting* perovskites, the high T_c copper oxides for example, conduction and magnetism share the same unpaired electrons in the same copper oxide layers. The competition between (super) conducting and magnetic insulating states is always important in interpreting their physical properties [34]. The coexistence of interesting conducting and magnetic properties is possible in this *molecular perovskite* in addition to a limited number of other molecular conductors [2–8].

3.2.4. Band structure

The low resistivity of this material is unique and interesting also in terms of its band structure. The extended Hückel tight-binding band calculation on this compound suggests that it should have two different types of bands; a quasi-1D band along the b^*-axis and a 2D band in the b^*c^*-plane (Fig. 6). As a result, this compound should have rather round and closed, i.e., 2D, Fermi surfaces in addition to narrowly closed but poorly warped, i.e., quasi-1D Fermi surfaces. The transport data and band structure calculations both are consistent with a localized system where electron correlations are significant. It is very intriguing whether $(ET)_3(MnCl_3)_2(C_2H_5OH)_2$ exhibits a superconducting transition when subjected to some thermodynamical condition change or perturbation. The study under way includes the electrical behavior under high pressure, under magnetic field, at lower temperature as well as syntheses of related new compounds.

4. Conclusions

$(ET)_3(MnCl_3)_2(C_2H_5OH)_2$ has been found to be a molecular "relative" of the perovskite-family. It is an

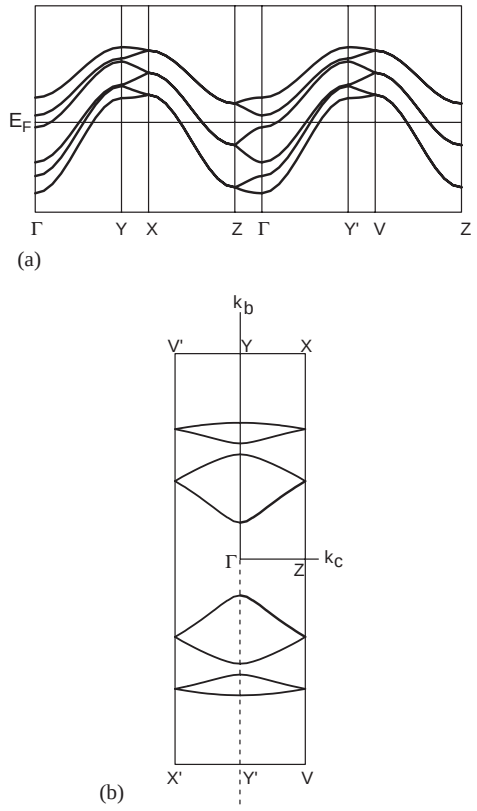

Fig. 6. (a) Calculated band structure and (b) Fermi surfaces. Γ, X, Y, Z and V correspond to (0,0,0), (0,1,1), (0,1,0), (0,0,1) and (0,−1,1), respectively.

organic–inorganic hybrid-type metallic conductor. Its unusual conducting and magnetic properties make it definitely worthy of further study.

Acknowledgments

We thank for the help of Dr. M. Wakeshima (Hokkaido University) in the magnetic susceptibility measurement. This work is partly supported by The Kurata Memorial Hitachi Science and Technology Foundation.

References

[1] T. Ishiguro, K. Yamaji, G. Saito, in: Organic Superconductors, 2nd Edition, Springer, Berlin, 1998.
[2] P. Day, M. Kurmoo, T. Mallah, I.R. Marsden, R.H. Friend, F.L. Pratt, W. Hayes, D. Chasseau, J. Gaultier, G. Bravic, L. Ducasse, J. Am. Chem. Soc. 114 (1992) 10722–10729.
[3] M. Kurmoo, A.W. Graham, P. Day, S.J. Coles, M.B. Hursthouse, J.L. Caulfield, J. Singleton, F.L. Pratt, W. Hayes, L. Ducasse, P. Guionneau, J. Am. Chem. Soc. 117 (1995) 12209–12217.
[4] H. Kobayashi, H. Tomita, T. Naito, A. Kobayashi, F. Sakai, T. Watanabe, P. Cassoux, J. Am. Chem. Soc. 118 (1996) 368–377.
[5] H. Kobayashi, A. Kobayashi, P. Cassoux, Chem. Soc. Rev. 29 (2000) 325–333.
[6] E. Coronado, J.R.G.-Mascaros, C.J.G.-Garcia, V. Laukhin, Nature 408 (2000) 447–449.
[7] R. Kato, Bull. Chem. Soc. Jpn. 73 (2000) 515–534.
[8] S. Uji, H. Shinagawa, T. Terashima, T. Yakabe, Y. Terai, M. Tokumoto, A. Kobayashi, H. Tanaka, H. Kobayashi, Nature 410 (2001) 908–910.
[9] T. Naito, T. Inabe, K. Takeda, K. Awaga, T. Akutagawa, T. Hasegawa, T. Nakamura, T. Kakiuchi, H. Sawa, T. Yamamoto, H. Tajima, J. Mater. Chem. 11 (2001) 2221–2227.
[10] T. Naito, T. Inabe, T. Akutagawa, T. Hasegawa, T. Nakamura, Synth. Metals 133–134 (2003) 445–447.
[11] (a) H. Miyasaka, Y. Yoshino, T. Ishii, R. Kanehama, T. Manabe, M. Yamashita, H. Nishikawa, I. Ikemoto, H. Kishida, H. Matsuzaki, H. Okamoto, J. Solid State Chem. 168 (2002) 418–426.
(b) R. Kanehama, Y. Yoshino, T. Ishii, T. Manabe, H. Hara, H. Miyasaka, H. Matsuzaka, M. Yamashita, M. Katada, H. Nishikawa, I. Ikemoto, Synth. Metals 9438 (2002) 1–2.
[12] T. Naito, T. Inabe, T. Akutagawa, T. Hasegawa, T. Nakamura, Y. Hosokoshi, K. Inoue, Synth. Metals 135–136 (2003) 613.
[13] (a) J.M. Williams, J.R. Ferraro, R.J. Thorn, K.D. Carlson, U. Geiser, H.H. Wang, A.M. Kini, M.-H. Whangbo, in: Organic Superconductors (Including Fullerenes), Prentice-Hall, Englewood Cliffs, NJ, 1992
(b) J.M. Williams, H.H. Wang, T.J. Emge, U. Geiser, M.A. Beno, P.C.W. Leung, K.D. Carlson, R.J. Thorn, A.J. Schultz, Prog. Inorg. Chem. 35 (1987) 51–218.
[14] (a) P. Batail, C. Livage, S.S.P. Parkin, C. Coulon, J.D. Martin, E. Canadell, Angew. Chem. Int. Ed. Engl. 30 (1991) 1498–1500.
(b) C. Coulon, C. Livage, L. Gonzalvez, K. Boubekeur, P. Batail, J. Phys. I (France) 3 (1993) 1153–1174.
[15] P. Day, in: A.K. Cheetham, P. Day (Eds.), Solid State Chemistry: Compounds, Oxford University Press, Oxford, 1992, pp. 37–38 (Chapter. 2).
[16] L.J. de Jongh, A.R. Miedema, Adv. Phys. 23 (1974) 1–260.
[17] T. Smith, S.A. Friedberg, Phys. Rev. 176 (1968) 660–665.
[18] M. Mekata, J. Phys. Soc. Jpn. 42 (1977) 76–82.
[19] R. Sessoli, H.-L. Tsai, A.R. Schake, S. Wang, J.B. Vincent, K. Folting, D. Gatteschi, G. Christou, D.N. Hendrickson, J. Am. Chem. Soc. 115 (1993) 1804–1816.
[20] H.J. Eppley, H.-L. Tsai, N. de Vries, K. Folting, G. Christou, D.N. Hendrickson, J. Am. Chem. Soc. 117 (1995) 301–317.
[21] T. Lis, Acta Crystallogr. B 36 (1980) 2042–2046.
[22] P. Batail, K. Boubekeur, M. Fourmigué, J.-C.P. Gabriel, Chem. Mater. 10 (1998) 3005–3015.
[23] A. Altomare, G. Cascarano, C. Giacovazzo, A. Guagliardi, M.C. Burla, G. Polidori, M. Camalli, J. Appl. Crystallogr. 27 (1994) 435.
[24] D.T. Cromer, J.T. Waber, International Tables for X-ray Crystallography, Vol. IV, The Kynoch Press, Birmingham, 1974 (Table 2.2 A).
[25] D.C. Creagh, J.H. Hubbell, in: A.J.C. Wilson (Ed.), International Tables for Crystallography, Vol. C, Kluwer Academic Publishers, Boston, 1992, pp. 200–206 (Table 4.2.4.3).
[26] L.J. Farrugia, J. Appl. Crystallogr. 30 (1997) 565 (the program is available from the following URL, http://www.chem.gla.ac.uk/~louis/ortep3/).
[27] T. Mori, A. Kobayashi, Y. Sasaki, H. Kobayashi, G. Saito, H. Inokuchi, Bull. Chem. Soc. Jpn. 57 (1984) 627–633 (the program is available from the following URL, http://www.op.titech.ac.jp/lab/mori/data.html).
[28] R. Dingle, M.E. Lines, S.L. Holt, Phys. Rev. 187 (1969) 643–648.
[29] B. Morosin, E.J. Graeber, Acta Crystallogr. 23 (1967) 766–770.
[30] T. Mori, Bull. Chem. Soc. Jpn. 72 (1999) 2011–2027.
[31] J.K. Burdett, Inorg. Chem. 32 (1993) 3915–3922.
[32] M. Matsuda, Thesis, Hokkaido University, 2001.
[33] G.R. Wagner, S.A. Friedberg, Phys. Lett. 9 (1964) 11–13.
[34] H. Fukuyama, S. Maekawa, A.P. Malozemoff (Eds.), Strong Correlation and Superconductivity, Springer, Berlin, 1989.